Bull. Spec. Astrophys. Obs., 1999, 48, 121-132

Reduction of Zeeman echelle spectra obtained with the SAO 1 m telescope

D.N. Monin

Special Astrophysical Observatory of the Russian AS, Nizhnij Arkhyz 357147, Russia

Received July 1, 1999; accepted July 14, 1999.

Abstract. Reduction of Zeeman echelle spectra taken with the coude spectrograph CEGS of the 1 m telescope of the Special Astrophysical Observatory for the programme of magnetic survey of the northern hemisphere main sequence stars is described. The reduction algorithms have been tested by the spectra of the magnetic Ap star 53 Cam (HD 65339).

Key words: stars: magnetic fields – instruments: echelle: CEGS – database: VALD – stars: individual: HD 65339

1. Introduction

In 1995 the work was initiated over carrying out a magnetic survey of northern sky main sequence stars up to $V = 4\overset{m}{.}0$. The aim of the survey is to construct a selection-independent function of distribution of main sequence stars on magnetic fields (see Bychkov et al., 1997). This kind of information would make it possible to compare magnetic properties of main sequence stars and evolved stars — white dwarfs. This survey can help to detect new magnetic stars. Part of the survey programme stars (approximately 1/3) have been measured by other authors with an accuracy of about 60–80 G with the purpose of detection of magnetic fields (Landstreet, 1982). However no significant magnetic field has been found in any of the objects. This suggests that either the magnetic field in them is actually absent, or it is less than 60–80 G. We are facing the problem of detecting and measuring magnetic fields with an accuracy as high as possible (better than 60–80 G). This requires high-quality spectra with a high signal/noise and mastering of new methods of high-accuracy determination of magnetic line shift in the spectra. During the period between 1995 and 1997 we obtained quality spectra for the majority of the magnetic survey stars with the coude-echelle spectrograph CEGS (Musaev, 1996). The description of the procedure of polarimetric observations with this device can be found in Bychkov et al. (1999). Therein one can also find the description of a polarimetric facility used to measure magnetic fields. The reduction of the data obtained called for the creation of algorithms for reduction of Zeeman echelle spectra. Some of the survey stars may show the presence of strong magnetic fields (over 1 kG). That is why, the algorithms must involve both a possibility of high-accuracy revealing weak magnetic fields and a possibility of detection of strong magnetic fields.

We present in this paper the full complex of procedures of reduction of spectral data obtained for the magnetic survey programme. We give also the results of reduction for comparison of our results with the results of other authors.

2. Principal reduction stages

The processing of the echelle spectra obtained with the polarimetric analyser is carried out in the MIDAS environment using the context ECHELLE (Balester, 1992). The particularities of these spectra require changes in most of the standard MIDAS procedures for reduction of echelle spectra. The spectra taken with the polarimetric analyser (hereafter referred to as Zeeman) consist from spatially separated (on the detector) spectra in two opposite circular polarizations (left circular polarization LCP and right circular polarization RCP).

This kind of reduction is distinct for the presence of closely spaced spectral orders in the LCP and RCP. Separation of the same orders in different polarizations is $4 \div 5$ pixels (this scatter will be discussed further in this paper), which is much less than the separation of adjacent orders in the same polarization, $15 \div 25$ pixels, and comparable with the order FWHM across the main dispersion (i.e. in slit height, along the Y-coordinate) which makes $2 \div 3$ pixels. A correct extraction of partially overlapping spectra in different polarizations is needed. An incorrect extraction may lead to a marked depolarization in the spectrum and thus to errors in the magnetic field value determination.

© Special Astrophysical Observatory of the Russian AS, 1999

Another distinction is that the presence of the polarimetric analyser in the optical path of the spectrograph causes complication of the dispersion curve. It follows from the equation of the grating that $m\lambda/d = \frac{X}{\sqrt{X^2+f^2}}$, where m is the absolute number of the order, d is the period of the grating, λ is the wavelength, f is the focal length of the camera, X is the coordinate in the dispersion plane recorded from the point of intersection of the camera axis with the detector plane. In the case where the camera focal length is much greater than the spectrum image size, $f \gg X$, the equation of the grating can be reduced to the form $m\lambda = aX + b$, where a and b are arbitrary constants. In our case such a relation poorly describes the real position of spectral lines.

The package of procedures in the MIDAS environment which we have written realizes the following stages of reduction of Zeeman echelle spectra:

- determination of the position of the orders;
- removal of particle hits;
- definition and subtraction of the background in the comparison spectrum image;
- extraction of echelle orders of the comparison spectrum;
- normalization and search for lines in the comparison spectrum;
- computation of the dispersion coefficients;
- removal of cosmic particle hits from the star spectrum image;
- the background subtraction in the star spectrum image;
- extraction of echelle orders of the star spectrum (separately for different polarizations);
- normalization and search for lines in the star spectrum (separately for different polarizations);
- linearization of the star spectrum;
- identification of lines;
- determination of magnetic shift of lines.

Some procedures, such as removal of cosmic particle hits, definition and subtraction of the background, extraction of echelle orders in the comparison spectrum are completely identical with those for the star image. The reduction of spectra is performed following exactly the sequence of the above procedures.

It is vital that for the high-accuracy reduction of polarization data the spectra should be taken in two positions of the entrance quarter-wave plate of the polarimetric analyser. In this case the LCP and RCP spectra switch places. Most of the instrumental effects, such as inclination of the slit projection to the dispersion direction in the spectrum, different sensitivity of different areas of the detector (CCD), inclination of the plane of splitting of the light beams in the analyser with respect to the spectrograph slit orientation (Bychkov et al., 1999).

When the plate is rotated by 90 degrees, the spectrum with the same state of polarization passes the same optical path in the spectrograph and is projected onto one and the same place on the detector. The position of the spectrum still varies a little because of the slightly different position of the object on the slit during the first and second exposures. Thus we obtain two spectra for each object (including the spectrum of the diffused solar light use as the comparison spectrum) with two positions of the quarter-wave plate differing by 90 degrees. The reduction of the two images is performed in an exactly the same way.

3. Searching for spectral orders

The search for the positions of spectral orders is made using a star spectrum with broad features (large $v \sin i$ values). There are practically no narrow lines in such objects, but for the terrestrial atmosphere lines that are located mostly in the orders of the spectrum with a smaller absolute number. The orders with large absolute numbers are practically free from the terresrial atmosphere lines. The absence of narrow lines in the spectrum makes it possible to reliably define the positions of spectral orders in the whole image. This allows the parameters of the polynomial that describes the position of spectral orders to be reliably determined. If there is no star spectrum with broad emission lines, one can use the scattered solar light spectrum. In this case the accuracy of determining the position of orders is somewhat worse.

Prior to the search for the position of orders the image is turned so that the wavelength increases in the image from left to right and from bottom upwards. One has to mirror the image about its central column. The median filtering of the image is further done only along the image columns (transverse the main dispersion) in a window of 10 pixels. This procedure results in marging of two closely spaced orders in opposite polarizations into one pseudo-order. This is done in order to subsequently find the position of spectral orders by using the standard MIDAS package. The MIDAS procedure of finding the position of spectral order implies a polynomial variation in the separation of orders and therefore it fails to describe the discontinuous function of variation in the separation of orders (two closely spaced orders in opposite polarizations, then two orders in opposite polarizations, but with the order number differing by 1). After that, applying the MIDAS procedure, determine the mask of the positions of the centres of orders. The number of the points corresponding to the given order in the mask may vary between 30 and 600 (depending on the spectrum quality and on the presence of narrow lines). The grid of positions can be fitted by a

two-dimensional polynomial of the 4th and 5th degree along the lines and along the columns, respectively. In the normal practice, one can find $35 \div 40$ pseudo-orders ($35 \div 40$ orders in the LCR and $35 \div 40$ orders in the RCP). This number depends on the quality of the spectrum used to find the position of orders. We found it a risk to extrapolate on the basis of the polynomial relation of such a high order (5th degree) in order to find additional, weaker orders. The more so, we were interested in spectral orders with reliable acquisition for high-accuracy measurement of magnetic fields. For this reason we used only these $35 \div 40$ orders found surely.

Proceeding from the two-dimensional polynomial that describes the positions of orders, a new mask is formed of the position of pseudo-orders with an equal step along the rows of CCD. The standard deviation of Y-positions of common points of the new and old mask is normally $0.04 \div 0.05$ pixel.

The position of the mask of pseudo-orders is displayed in Fig. ??. The figure shows the position of mask nodes with a step of 50 pixels along the dispersion in three parts of the echelle-spectrum image of the star α Aql: at the centre, left and right edges. The picture is magnified approximately 10 times in the direction normal to that of extension of orders. It can be seen that the position of the mask nodes describes well the position of intersection of the spectra in the LCP and RCP.

In the case the star spectrum with a large $v \sin i$ acquired during the night is lacking, we use the spectrum of the scattered solar light to find the position of orders. The spectrum is rich in narrow and deep lines, therefore the accuracy of construction of the mask turns out to be somewhat worse, $0.08 \div 0.1$ pixel. On the whole, a high acquisition (a signal-to-noise ratio over 100) and the same optical path through the spectrograph are vital for correct location of spectral orders.

The latter condition is not fulfiled in the case of use of a tungsten lamp. The difference in the position of the mask nodes obtained from the star spectrum with a large $v \sin i$ and from the lamp is shown in Fig. ??. The difference is shown for each order as a separate continuous curve. It can be seen that the difference for individual orders may reach 2 pixels. For this reason we do not use the tungsten lamp to find the position of orders.

The grid of the positions of spectral orders is further used to construct a mask of the position of spectral orders in the LCP and RCP. The procedure will be described below.

4. The comparison spectrum

As the comparison spectrum, we normally use the spectrum of the scattered solar light, which we acquired immediately before and after the observations. For this purpose we expose an arbitrary area of the morning or evening sky, the telescope being immovable. The diffused sky light, as well as the light of the object, passed through the polarimetric analyser. It fills the slit completely, and therefore does not give spatially separated spectra of the LCP and RCP. The given spectra overlap, forming a common profile of an order across the main dispersion (Fig. ??, dotted line).

5. Removal of cosmic particle hits

The removal of cosmic hits in the image was done in the following manner. Filtering of every line of the image in a window of 10 pixels was performed. At this extent no inclination of spectral orders by more than 1 pixel occurs (an inclination of 1 pixel in the cross dispersion plane takes place only within 20 pixels along the main dispersion). This window is also large enough for narrow and deep lines having a large intensity gradient in the wings. With a large gradient in most of the pixels of the window, the median value will be considerably different from the value in a certain pixel of the window even if there is no cosmic hit. This is why, with this kind of filtration we can miss high intensity traces of cosmic hits oriented along the rows of the image. This occurs when the extent of a particle trace in the direction parallel with the rows is comparable with the size of the window or above it. Such particle traces are not cleaned at this step, but their presence is analysed in a one-dimensional spectrum. This kind of particles make up no more than $1 \div 2\,\%$. An example of the clearing procedure is shown in Fig. ??. In the figure is presented a small portion of the image before and after the clearing. It can be seen that the particle traces well localized and of small extent in the direction parallel with the lines of the image are cleared very well. The only trace with a size of 10 pixels was not removed. When filtering for the median flux changed only in the pixels in which it was different from the median value in a window by a value multiple of the standard noise deviation in the case of Poisson noise distribution: $I - I_{median} > n\sqrt{I_{median}}$, where I, I_{median} is the flux in the given pixel of the original image and the image after the median filtration was applied, respectively. Parameter n varied from image to image within $2 \div 5$. When the line width in the stellar spectra increases, the gradient in the wings usually drops. This is why, the algorithm works well with both narrow-line stellar spectra and broad-line stellar spectra. The procedure is checked by analysis of the difference of the two images: before and after the removal of particles.

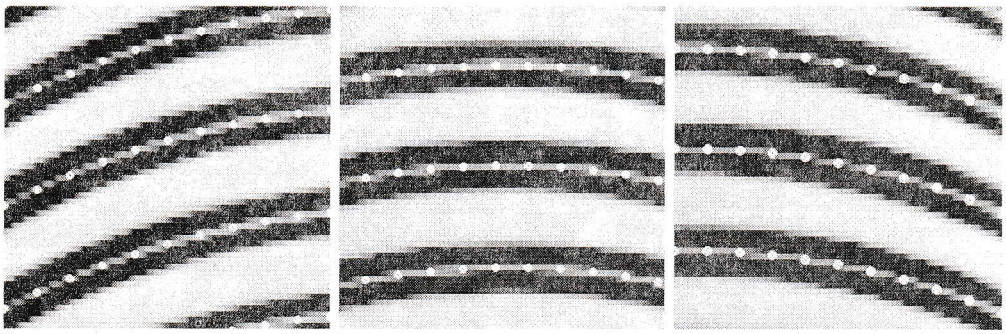

Figure 1: *Position of the mask of pseudo-orders (white dots) of the left edge, at the centre, and at the right edge of the image. Small fragments are shown of individual portions of three central spectral orders in LCP and RCP (in black).*

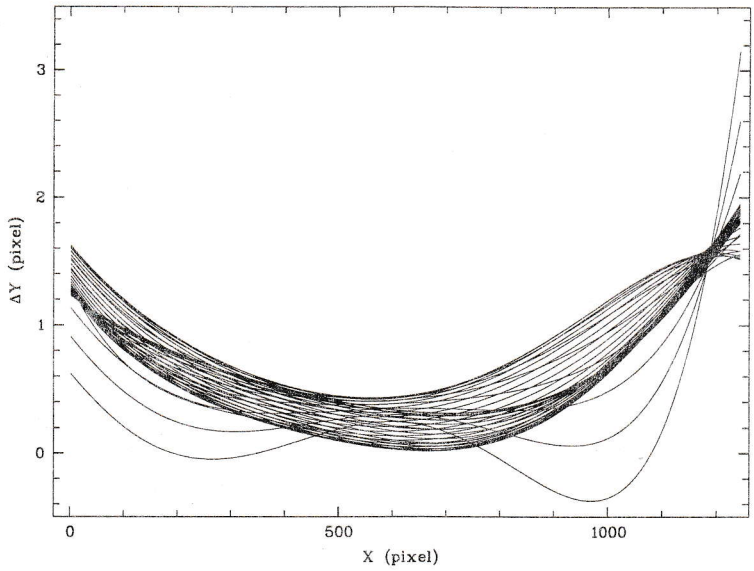

Figure 2: *Difference in the position of the mask modes in the cross-dispersion plane vrs the position in the main dispersion plane. An individual curve corresponds to each spectral order.*

6. Background subtruction in the image

For proper extraction of the point source spectrum from the echelle spectrum correct account of the scattered light in the spectrograph ought to be taken. It is variable over the image and may vary within $2 \div 10$ percent of the intensity in the nearest spectral order.

Based on the mask of the positions of pseudo-orders, a mask of location of the background points is constructed. The points of the background mask take up a position along the columns of the image which is equidistant from two nearest centres of pseudo-orders. The imaging of the background is realized through describing the points in the background mask by splines of the 3rd degree along the image columns. The step in the background mask along the lines of the image is 1 pixel. To minimize the influence of the background fluctuations, the intensity in each point of the background mask is considered to be an average of the intensities in the nearby pixels (in the vicinity of the central pixel). This vicinity is determined by a rectangle of side of 7 pixels along the main dispersion and 3 pixels transverse it. The size of the vicinity is chosen for the following reasons. Along the main dispersion the bending and inclination of orders must not have an effect on the result of averaging, while transverse the main dispersion the vicinity must be much smaller than the separation of orders in different polarizations with the number of the order differing by 1.

Fig. ?? shows the cross-section of the Zeeman echelle image of a stellar source across the main dispersion. The cross-section of the background image is superimposed there also. Prior to the sub-

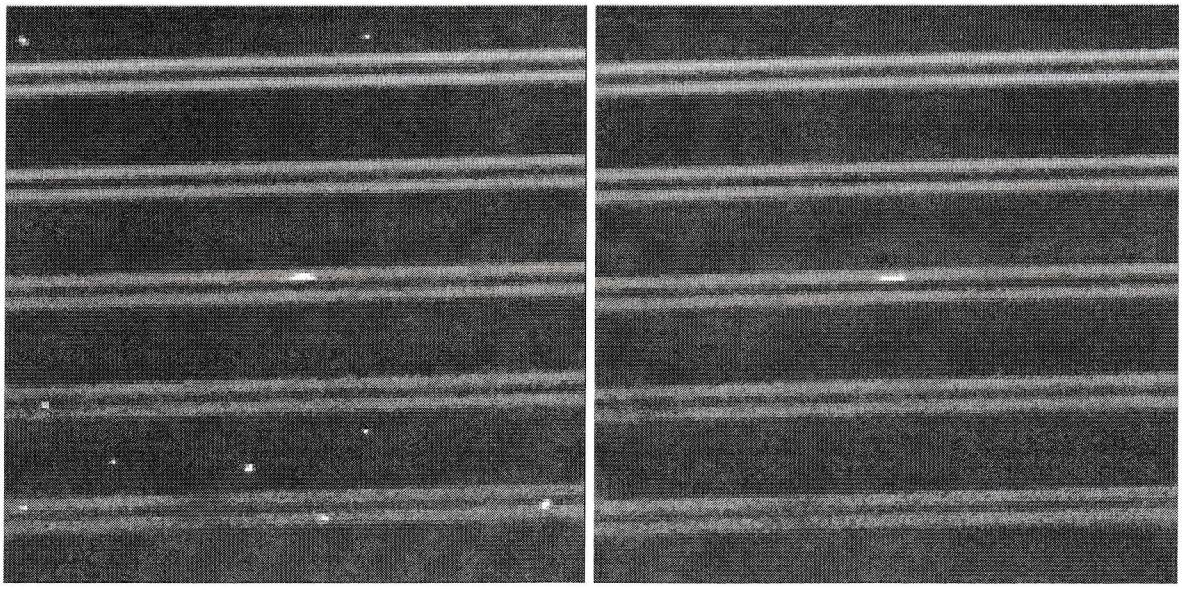

Figure 3: *Example of operation of the procedure of clearing the image from cosmic hits. The left panel is the image prior to clearing, the right one is that after clearing.*

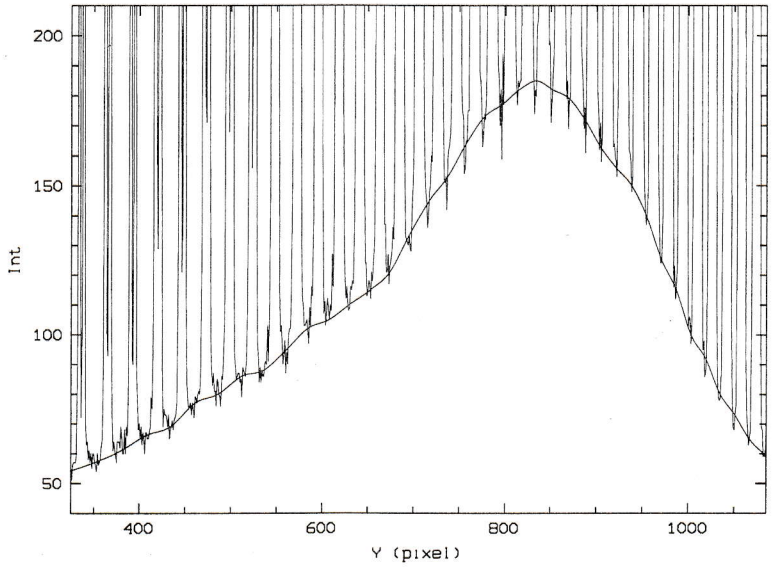

Figure 4: *Section of a Zeeman echelle image of a stellar source transverse the direction of extension of spectral orders. The section of the background light image is superimposed. The Y axis is the intensity in ADU units.*

traction the background in the interorder space is $20 \div 200$ ADU/pixel and has a rather complex profile. The intensity of the residual light in the interorder space after the subtraction of the background is less than 2 ADU/pixel with a standard noise deviation in the interorder space of 4.3 ADU/pixel. Thus after the subtraction of the background the interorder space becomes a plane with the mean value equal to zero within the noise statistics.

7. Extraction of echelle orders

In Fig. ?? is displayed a portion of the echelle spectrum of the star αBoo normal to the main direction of dispersion (solid line) and also a similar section of the comparison spectrum, in this case the section of the scattered solar light spectrum (dotted line). The intensity of the scattered solar light spectrum is increased by a factor of 10. The figure shows only a part of the section that contains three spectral or-

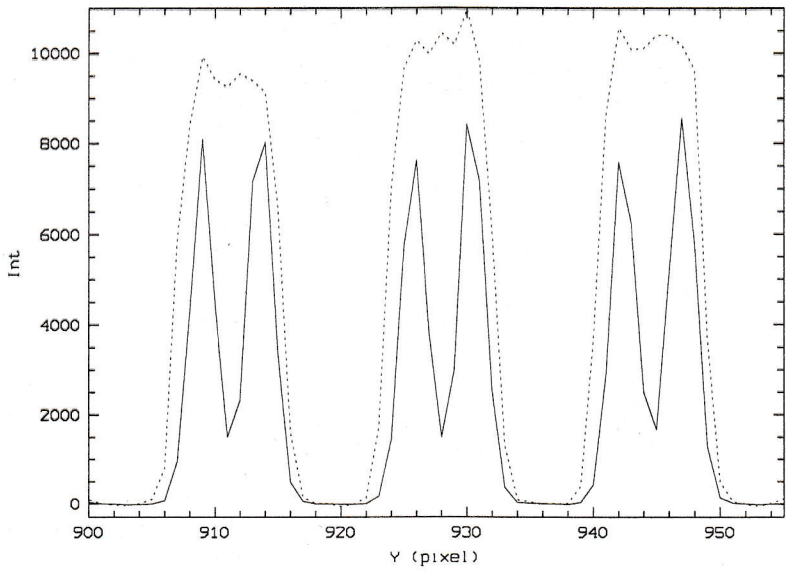

Figure 5: *Portion of the section of the echelle spectrum of the star αBoo normal to the main dispersion direction (solid line) and a similar section of the scattered solar light spectrum (dotted line). The Y axis is the plot of intensity in ADU units.*

ders. The orders in the star spectrum in the LCP and RCP overlap one another.

The extraction of spectral orders is performed on the basis of the mask of the position of pseudo-orders. The slit position on the Y-coordinate (along the cross-dispersion direction) with respect to the centre of the pseudo-order is specified interactively. The lower and upper boundaries for the extraction of spectral orders in the LCP and RCP are specified separately. An important point is that the same boundaries of extraction are used for a pair of spectra of one and the same object obtained with different positions of the entrance quarter-wave plate.

The mask for the extraction of orders in the LCP (RCP) is formed on the basis of the mask of pseudo-orders by means of introduction of a shift in the cross-dispersion plane. The shift is a constant for the given order and changes from order to order. The shift of the order in the LCP (RCP) with respect to the pseudo-order varies from order to order for two reasons: variation of magnification by cross-dispersion prism and insufficient achromatism of the polarization analyser.

From the spectra with a S/N>100 we have examined how the distance between the maximum concentration in the cross-dispersion plane in the LCP (RCP) and the maximum concentration in the pseudo-order as well as the separation of orders in the LCP and RCP change throughout the image.

The centre-to-centre distance of the spectrum in the LCP (RCP) and the pseudo-order changes mainly because of the difference in filling the slit by the comparison spectrum (scattered light of the Sun) and the spectrum of the object. The comparison spectrum fills the slit completely. The variation is not above 0.1 pixel and we neglect it.

The distance relation between the orders in the LCP and RCP is presented in Fig. ??. It is seen from the figure that the separation of the orders in the LCP and RCP is clearly dependent on the wavelength. The solid line shows approximation of the points by a 3rd degree polynomial. The fact that the main contribution to the variation in distance between the orders with different states of polarization is made by the variation of angular magnification on the prism is confirmed by the increase in the FWHM of the order profile in the LCP (RCP) along the cross-dispersion when going to orders with a smaller absolute number. The FWHM changes by about a factor of 1.3 at order edges, which is consistent with the amplitude of variation in separation of orders in the LCP and RCP on the edges of the spectral range (see Fig. ??). The FWHM of individual unblended lines on edges of the spectral range at $\lambda 4000 - 9000$ practically does not change, which suggests that the focusing is good over the whole image.

The contribution to the variation of separation of orders in LCP and RCP caused by the insufficient achromatism of the polarization analyser is insignificant, if at all.

We use the relationship presented in Fig. ?? to calculate the displacement of the mask of pseudo-orders

for extraction of orders in LCP and RCP.

In spectra of high quality the mask of positions is found from the spectrum of the object itself, separately for the spectrum in the LCP and RCP (the mask of positions of pseudo-orders is used as a first approximation). The positions of the centres of orders in LCP and RCP are determined by fitting a gaussian transverse the main dispersion direction at different points of the order.

For objects with low S/N spectra the limits of extraction of spectra of both polarizations (the position and size of the slit projection on the detector in LCP and RCP separately) were specified interactively for each object, or on the basis of the mask of position of spectra in the LCP and RCP obtained from spectra with a high S/N ratio, or using the relationship given in Fig. ??. Usually a mask obtained once a night is used for extraction of all objects of the given night or, at least, for extraction of a pair of spectra of one and the same object obtained with different position of the entrance quarter-wave plate of the polarization analyser. For different objects only a minor common displacement of both masks (the mask of the spectrum in LCP and RCP) due to somewhat different positions of objects on the slit of the spectrograph is introduced. The slit length to isolate spectra of the given polarization depends on the quality of the object image and ranges from 5 to 7 pixels. A detailed description of the integration procedure can be found in Ballester (1992).

8. Normalization of the spectrum

The normalization of the spectrum was performed in two ways interactive and automatic. The automatic construction of the continuum was based on the algorithm of convolution of the spectrum with a gauss-like window. The algorithm is implemented in the form of MIDAS procedure (Shergin et al., 1996). The automatic way is good for objects with narrow enough lines in the spectrum (with a full width at the line base of about 40 pixels). The interactive construction of the continuum required specification of a number of points in every spectral order. The points were smoothed by a 3rd-degree spline for each order. All the points can be edited (add or removed) in striving for a maximum likeness of normalized spectra in the LCP and RCP in the continuum.

In objects with broad lines (taking sometimes more than half of the spectral order) the shape of the continuum was reconstructed by the spectrum of a tungsten lamp taken on the same night. Lines in the spectrum of the lamp are missing practically in the whole spectral range. This is a rough procedure and therefore used but in the spectra with broad lines, where it was difficult to reconstruct the continuum shape. In our further studies we contemplate to introduce an algorithm of construction the continuum in an order containing broad emission lines, reconstructing it by interpolation of intensities in the nearby orders which do not contain significant spectral features.

8.1. Searching for lines in the spectrum

Searching for lines in the comparison spectrum follows the standard MIDAS procedure. This procedure becomes inefficient only in the case of broad lines whose width is over 40 pixels. In this case interactive search for lines can be implemented, making it possible to locate a line detected, delete mistaken line or redetermine its position. Two cases of finding lines are possible: separately for the LCP and RCP spectrum and on the summarized spectrum. One or the other procedure is applied depending on the spectrum quality, on the presence or absence of noticeable magnetic splitting of lines, total number of lines in the spectrum.

When identifying lines in spectra of different polarizations separately by means of an additional procedure, one and the same line on both spectra with a possible shift with respect to each other due to the slit inclination or caused by the presence of a magnetic field is further identified.

This operation may result in incorrect identification, for this reason it is checked interactively. Close lines whose centre distance is comparable with their width are considered blended and are excluded from further use. In spectra of stars of different spectral classes and with different $v \sin i$ values, it is possible to detect from a dozen to a few thousand lines.

8.2. The dispersion relation

The dispersion relation is constructed from the spectrum of the scattered solar light. The sum spectrum in the LCP and RCP is used for that. The laboratory wavelength is specified for no less than 20 lines with the use of the list of solar spectrum lines of Pierce and Breckinridge (1973). Use is made of the solar spectrum lines. The terrestrial atmosphere spectrum lines are discarded, since further one has to introduce a correction in the solar spectrum line shift due to the rotation of the Earth. The shift varies within $-0.3 \div +0.3\,\mathrm{km/s}$. This effect taken into account, the line position remains constant both during the night and between different nights of one run within measurement accuracy.

The search for the dispersion relation has the form $\lambda_{lab} m = F(X, m, \alpha)$ where λ_{lab} is the laboratory wavelength, m is the absolute number of the spectral order, X is the X coordinate of the line, α is the angle of rotation of the image. Angle α is determined from the examination of the solar spectrum

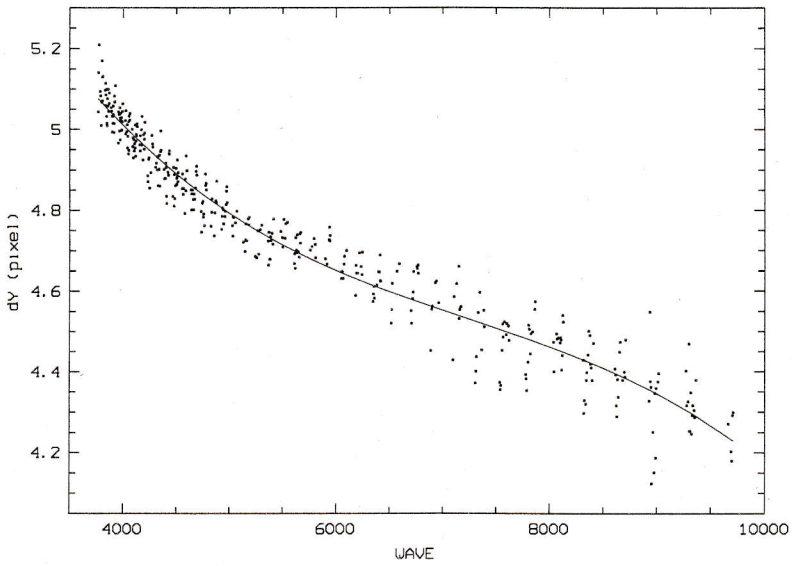

Figure 6: *Separation of orders in LCP and RCP as a function of wavelength (angstroms). The solid line is the approximation of the points by a 3rd degree polynomial.*

lines in the LCP with respect to those in the RCP. Typically the angle fluctuates within $0 \div 5°$. This parameter can be obtained with an accuracy $0.2 \div 0.3°$. The accuracy of construction of the dispersion relation is $0.004 \div 0.010$ Å. This appears sufficient to reliably identify spectral lines. The accuracy in determining the dispersion relationship does not affect that of magnetic field measurement because we make differential measurements of the magnetic line shift. Even with the strongest magnetic fields, the line shift is no greater than a few Å. At the same time magnetic field dependence on wavelength is very weak and does not show up itself in short wavelength region.

8.3. Wavelength calibration of the stellar spectrum

The wavelength calibration of the median position between the centres of one and the same line present in the LCP spectrum and RCP spectrum is performed with the aid of a two-dimensional dispersion relation. The position of one and the same line in different polarizations may be different because of magnetic splitting. However, the centre between one and the same line in different polarizations represents (by virtue of symmetry of the splitting pattern) the position of the unshifted spectral line component. The reciprocal linear dispersion was calculated in the vicinity of the unshifted component of every line in the spectrum.

All measurements in the spectrum are made without linearization of the entire spectrum, only the positions of the unshifted component of every line are converted into wavelengths. This is done in order to avoid distortion of the line profile. These distortions may occur when rebinning to equal wavelength steps (see Mathys, 1991).

The wavelengths of the unshifted components of the Zeeman splitting are further identified with those of different chemical elements.

8.4. Line identification

Prior to line identification in the object spectrum the average Doppler shift was corrected for Earth's rotation and orbital motion. As a first approximation, we use the radial velocity value from the BSC catalogue (Hoffleit, 1982). Subsequently, the total shift due to the radial velocity is varied interactively to provide the best identification and lack of wavelength dependence of deviations of identified lines' positions from those of lines from the list. Correctness of identification is checked visually in different parts of the spectrum. For spectral line identification we use the list of lines formed by the database VALD (Piskunov et al., 1995). The list of lines is formed in accordance with the basic parameters of a stellar atmosphere (temperature, gravity, microturbulent velocity, chemical composition). Those parameters for every object are taken from the literature. Then the list of the lines identified in the spectrum is compared with the list of lines retrieved from the database. In addition, the terrestrial atmosphere lines, which undergo no significant shift due to the radial velocity, are identified. The given list of lines was issued on the base of the list of Pierce and Breckinridge (1973). Such lines number 1868 in the wavelength range $\lambda 4000 - \lambda 9000$. These

lines are utilized to inspect the results obtained.

8.5. Magnetic field measurement

The presence and magnitude of magnetic field are analysed from the line profile shift in one circular polarization with respect to the other. In the presence of a magnetic field a spectral line with a wavelength λ_0 is split into several components. In transition between sublevels for which $\Delta M = 0$, where M is the projection of the total angular moment onto the magnetic field direction, π components form. Transition with $\Delta M = \pm 1$ give σ components. The splitting value is determined by the expression

$$\Delta\lambda = \pm 4.67 * 10^{-13} g H \lambda_0^2, \quad (1)$$

where $\Delta\lambda$ is measured in Å, g is the Lande factor of the transition, H is the magnetic field strength expressed in G (see Landstreet, 1980). Since the scale of splitting of different levels is unequal, the number of components will depend on the electron configuration and may reach a few dozens. The components of splitting are polarized. When observing transverse the magnetic field sense, π components turn out to be linearly polarized parallel to the field, while σ components are linearly polarized across the field. When observing along the field direction, σ components exhibit the opposite circular polarizations. In isolating separately the left and right circular polarizations, we recorded a totality of the line components with the same circular polarization states. It should be noted that linearly polarized light of a star enters equally into both the left circularly polarized spectrum and the right circularly polarized one.

In weak magnetic fields (a few kilogauss or more) the scale of splitting turns out to be over an order of magnitude less than the spectral resolution of the spectrograph. In this case we do not see the components of splitting taken separately, but see the total profile they form. The centre of gravity of this summarized profile in the LCP and RCP spectrum (λ_L and λ_R) is displaced with respect to λ_0 by

$$\Delta\lambda_{L,R} = \lambda_{L,R} - \lambda_0 = \pm 4.67 * 10^{-13} < g > H_l \lambda_0^2, \quad (2)$$

where $< g >$ is the profile weighted mean Lande factor, H_l is the longitudinal magnetic field or the projection of the magnetic field component averaged over the visible hemisphere of the star on the line of sight (Mathys, 1987, 1991). The "+" sign in the formula corresponds to the RCP. Not the line profile shift in the LCP or RCP with respect to λ_0 is measured, but the mutual displacements of the profiles:

$$\Delta\lambda = \lambda_R - \lambda_L = 9.34 * 10^{-13} < g > H_l \lambda_0^2. \quad (3)$$

It should be emphasized that we measure the centres of gravity of the profiles with different state of polarization in the non-linearized spectrum. The linearization procedure is applied only to the wavelength determination of the line centre found. This is done for the purpose of avoiding distortion of the profile in this procedure, which could result in incorrect determination of the position of the line centre of gravity. The wavelength of the line centre can be found from the dispersion relation derived above. The line centre of gravity in the LCP and RCP can be found in a standard way:

$$X_{L,R} = \frac{\int R_c^{(L,R)}(X) X dX}{\int R_c^{(L,R)}(X) dX}, \quad (4)$$

where X is the coordinate of a given point of the profile expressed in pixels, $R_c^{(L,R)}(X)$ is the residual intensity of the profile in the LCP and RCP, respectively. Further, in accordance with the dispersion relation, these positions of the centres of gravity are converted to wavelengths.

The effective Lande factors of lines can be obtained using the database VALD. The lines, for which the effective Lande factor was unknown, were excluded.

8.6. The influence of various instrumental effects

The determination of the shift of the profile centre of gravity in one polarization with respect to that in the other is largerly affected by quite a number of instrumental effects. Among these are the effects of depolarization of radiation and spurious polarization of light when it passes through the mirrors of the telescope and spectrograph. These effects have been examined by Bychkov et al. (1998). They have been shown to be insignificant. To quote Bychkov (1999), depolarization does not exceed $1 \div 2$ %. These effects change appreciably only in large wavelength intervals and may be neglected in differential measurements of the shift within the profiles of stellar lines. The widest lines have a full width of a few dozen angstroms, while the effects of depolarization and additional polarization of radiation change markedly throughout the spectrum on scales of thousands of angstroms. As it will further be shown, our work confirms these conclusions. The good agreement of the magnetic field strengths of the star 53 Cam at different phases of the period of rotation suggests that even if the above effects are present, they are negligibly small in the case of differential measurements of the line shift.

Another effect consists in additional shift of the profiles in the LCP and RCP due to the monochromatic inclination of the slit image with respect to the direction of the main dispersion in the spectrum. A detailed description of the effect can be found in Bychkov et al. (1999). For instance, a slit inclination of

4° results in an additional shift of 0.5 pixel. It should be emphasized that the shift of the profiles in the LCP and RCP of 0.5 pixel around $\lambda 6000\,\mathring{A}$ corresponds to a magnetic field of ≈ 1200 G. The slit inclination angle with a given configuration of the spectrograph is determined in the procedure of deriving the dispersion relation and checked by the spectrum lines having a great extent transverse the dispersion direction in the spectral order (about 15 pixels). The accuracy of determination of the inclination angle in this way makes $0.2 \div 0.3°$. This corresponds to an additional shift of $0.02 \div 0.03$ pixel in the spectrum of a star-like object, which is comparable with the accuracy of determination of the line centre of gravity.

By virtue of a number of causes to which the residual aberrations of the spectrograph optics can be referred, the inclination of the slit image with respect to the dispersion direction changes in different parts of the echelle frame and may differ by about $1.5 \div 2.0°$, which corresponds to a shift of 0.15 pixel. For this reason for high-accuracy measurement of magnetic field we apply a method of comparison of shifts of line profiles in the LCP and RCP on two independent echelle frames. These echelle spectra were obtained immediately following one another during the night with different positions of the entrance quarter-wave plate (Bychkov et al., 1999). When measuring the plate position the LCP and RCP spectra interchange the position on the detector, and therefore the magnetic shift (line profile shift in the LCP and RCP caused by the magnetic field presence) reverses its sign. At the same time, the shift caused by the slit inclination does not change the sign. Thus, the magnetic shift can be isolated from two exposures taken with different positions of the quarter-wave plate in the following manner: $\Delta\lambda = (\pm\Delta\lambda_2 \mp \Delta\lambda_1)/2$, where $\Delta\lambda_{1,2}$ is the shift of the LCP and RCP line centres of gravity in the 1st and 2nd exposures, respectively. The signs are taken in accordance with the true mutual positions of spectra of different polarizations on the detector. If the LCP spectrum is located on the detector closer to the upper end of the frame as compared with the RCP spectrum, the upper signs of the expression should then be used. The spectral orders having the smaller absolute number are located at the upper end of the echelle frame. The given expression specifies the field sign. The true mutual positions of the LCP and RCP spectra are checked by spectra of magnetic stars which do not change the sign during the whole period of rotation. For this purpose we analyzed the spectrum of the magnetic star BX Boo (HD 133029) that shows a nearly constant positive magnetic field of $+3500 \pm 600$ G.

The magnetic field is determined by expression (3). In so doing, all the identified lines in the spectrum of the given star, for which the effective Lande factors are known, are used. In the determination of the magnetic field the line weights are employed. The line weight is determined by the residual line intensity at the centre of gravity $w = (R_c^{(L)}(X_L) + R_c^{(R)}(X_R))/2$ For n lines with a magnetic field intensity $H_l^{(i)}$ and weight w_i, the magnetic field is determined as follows:

$$H_l = \frac{\sum_{i=1}^{n} H_l^{(i)} w_i}{\sum_{i=1}^{n} w_i}. \tag{5}$$

The magnetic field determination error is computed according to the following expression:

$$\sigma_{H_l} = \frac{\sqrt{\sum_{i=1}^{n} (H_l^{(i)} - H_l)^2 w_i^2}}{\sum_{i=1}^{n} w_i}. \tag{6}$$

8.7. Test of the algorithms of reduction and magnetic field determination

To check the correctness of operation of all the algorithms, the magnetic field has been measured from the spectrum of the magnetic star 53 Cam at different phases of the period of rotation. The spectra were taken on March 6–7 and April 3–4, 1999. Four Zeeman echelle spectra of the star were obtained in each of the two runs (two spectra with one position of the quarter-wave plate and two with another position differing by 90°). 53 Cam (HD 65339) is a well-known Ap star with a strong magnetic field. The longitudinal component of the field varies from −5 to +5 kG with a period of 8.02681 days (Hill, 1998). The star has a stellar magnitude $V = 6^m.01$. Spectra of satisfactory quality were obtained (with a S/N ratio of 20–50 in the range $\lambda 5000 \div 6500$). The spectrum is reach in narrow lines because of the low rotation velocity and numerous lines of different elements. The magnetic field of the star during the first observing run must have been (according to Hill, 1998) close to the phase of the positive extremum, while during the second run we must have observed the magnetic field sign change. We have processed in a similar manner all the available spectra, using the procedure described in this paper. The list of lines for identification of different spectral features and determination of their Lande factors has been drawn using the database VALD. The following physical parameters for 53 Cam have been used: $T_{eff} = 8500K$, $\log g = 4.2$, the microturbulent velocity is 2 km/s (Adelman, 1985; Michaud et al., 1981). The radial velocity of the star, −5 km/s, has been adopted from the catalogues BSC.

Because of the complexity of the pattern of splitting, about 90 lines have been identified in the spectrum, 20–30 of which have been selected as unblended. The majority of these are the lines of FeI (70 %), the rest of them are the FeII lines (30 %).

To exclude the instrumental effects, the magnetic field measurement has been performed from a pair of images obtained one after the other with different positions of the entrance quarter-wave plate.

Table 1: *Results of magnetic field measurements in 53 Cam*

JD (2451200+)	Phase	T_{exp}, min	H_l, G	n	σ_{H_l}, G
44.4028	0.131	30	3300	28	340
44.4312	0.134	30			
44.4562	0.137	30	3700	27	340
44.4799	0.140	30			
72.2653	0.602	40	-2500	23	160
72.2979	0.606	40			
72.3576	0.613	40	-2800	14	330
72.3896	0.617	40			

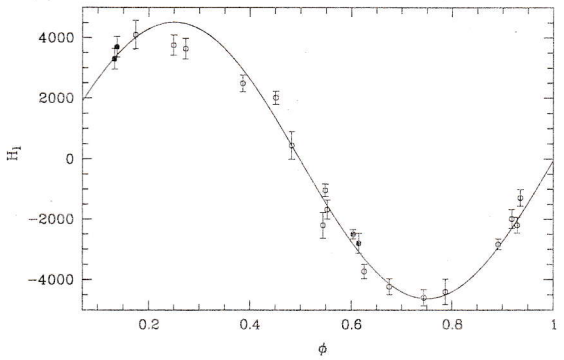

Figure 7: *Magnetic field variation of 53 Cam vrs phase of rotation. On the Y axis is laid off the longitudinal magnetic field H_l (gauss). The open circles represent the data obtained by Hill (1998). The solid line is the approximation by a sinusoid. The filled circles indicate our measurements. The vertical bars show the magnetic field measurement errors.*

The measurement results are presented in Table 1. In the first column are given the Julian dates of the middle of the exposure for each pair of spectra. The second column are the phases of the period of magnetic field measurement computed according to the ephemerides from Hill (1998). In the third column are listed the lengths of the exposures, the fourth column presents the longitudinal magnetic field calculated by expression (3), the next are the number of lines used and the error of longitudinal magnetic field determination.

The variation of the magnetic field of 53 Cam vrs phase is shown in Fig. 7.

Our results of magnetic field determination in 53 Cam are seen to be in good agreement with the data of Hill (1998) in spite of the difference in the techniques (Hill used a polarimeter measuring the degree of polarization in the wings of the hydrogen line $H\beta$) and of the fact that the field has been determined from lines of different elements.

For brighter objects from the programme of magnetic survey, for which the S/N ratio in the spectra turns out to range from 100 to 200 and in which the strong magnetic field and therefore the complex line splitting are lacking, we may expect a much better accuracy of magnetic field measurement, up to 10–20 G. It is this accuracy that we attain when measuring the magnetic field in the scattered solar light spectrum.

9. Conclusion

Algorithms for reduction of spectral data obtained for the programme of magnetic survey of northern sky main sequence stars have been implemented. Similar algorithms are meant for detection of weak magnetic fields (as weak as 10–20 G) in bright main sequence stars, up to $V = 4^m$. Such a good measurement accuracy is provided for by the high resolution, $R = 40000$, of the spectrograph CEGS, high quality spectra, high stability, as well as the possibility of magnetic field measurement from a great number of spectral lines (to a few thousands) with the use of the most accurate data on the Lande factor from the automatic database VALD. The correctness of the derived magnetic field strengths has been shown by comparison with the data of other authors. In particular, the magnetic field magnitude of the Ap star 53 Cam at different phases of magnetic field variation has been found to check with Hill's (1998) data.

Acknowledgements. The author expresses gratitude to Fabrika S. N. for help in definition of the problem both at the stage of preparation of the work and at the stage of discussion of the results, for assistance in seeking for a correct strategy of reduction. The author thanks Bychkov V. D. for discussion of the paper and individual reduction algorithms and for useful data on depolarization of radiation at the 1 m telescope of SAO RAS. I should like to thank also Romanyuk I. I. and Valyavin G. G. for helpful discussions and for observing (Valyavin) the star 53 Cam, Kasatenko I. V. for help in preparation of the paper. The work was supported by grant of the programme "Spectral survey of northern sky stars up to 5^m".

References

Adelman S.J., 1985, Publ. Astr. Soc. Pacific, **97**, 970

Ballester P., 1992, ESO/ST-ECF Data Analysis Workshop, 177

Bychkov V.D., Monin D.N., Fabrika S.N., Valyavin G.G., 1997, Stellar magnetic fields, eds.: Yu. V. Glagolevskij and I. I. Romanyuk, 124

Bychkov V.D., Romanenko V.P., Bychkova L.V., 1998, Bull. Spec. Astrophys. Obs., **45**, 110

Bychkov V.D., Galazutdinov G.A., Musaev F.A., Naidenov I.D., Panchuk V.E., 1999, (in press)
Bychkov V. D., 1999 (private communication)
Hill G.M., 1998, Mon. Not. R. Astron. Soc., **297**, No.1, 236
Hoffleit D. (with the collaboration of Jaschek, C.)), 1982, The BRIGHT STAR CATALOGUE, 4th revised edition (New Haven: Yale University Observatory)
Landstreet J.D., 1980, Astron. J., **85**, n.5, 611
Landstreet J.D., 1982, Astrophys. J., **258**, 639
Mathys G., 1988, Astron. Astrophys., **189**, 179
Mathys G., 1991, Astron. Astrophys. Suppl. Ser., **89**, 121
Michaud G., Megessier C., Charland Y., 1981, Astron. Astrophys., **103**, 244
Musaev F.A., 1996, Pis'ma Astron. Zh., **22**, No.5, 715
Pierce A.K., Breckinridge J.B., 1973, KPNO Cont. No. 559
Piskunov N.E., Kupka F., Ryabchikova T.A., Weiss W.W., Jeffery C.S., 1995, Astron. Astrophys. Suppl. Ser., **112**, 525
Shergin V.S., Kniazev A.Yu., Lipovetsky V.A., 1996, Astron. Nachr., **317**, No.2, 95